

光学学报

基于双光子聚合3D打印的光纤法珀微波导腔制备及传感特性研究

陈茂庆^{1,3*}, 刘思源^{1,3}, 蔡露^{1,3}, 刘强^{1,3}, 赵勇^{1,2,3**}

¹东北大学信息科学与工程学院, 辽宁 沈阳 110819;

²东北大学流程工业综合自动化国家重点实验室, 辽宁 沈阳 110819;

³河北省微纳精密光学传感与检测技术重点实验室, 河北 秦皇岛 066004

摘要 将光纤法布里-珀罗(法珀)微腔与微波导相结合, 提出一种光纤法珀微波导腔高灵敏度折射率传感器。光纤法珀微腔可以将光场限制在微米量级的区域内, 并对腔内的微波导结构起支撑保护作用; 微波导在保证结构良好导光能力的同时, 基于其强倏逝场特性, 进一步提升整体结构的折射率灵敏度。此外, 基于飞秒激光双光子聚合高精度3D打印技术, 可实现波导直径仅为2 μm的光纤法珀微波导腔, 并保证良好的制备重复性。实验结果表明: 随着光纤法珀微波导腔传感器腔内液体折射率的增加, 传感器的干涉光谱发生蓝移, 在1.3346~1.3764折射率范围内灵敏度可达525.81 nm/RIU, 与仿真获得折射率灵敏度(555.14 nm/RIU)结果接近; 该传感器还展现了优良的线性响应特性, 线性拟合系数可达0.9948; 相比于传统无微波导的光纤法珀微腔结构, 干涉光谱峰值提升了8.2 dB, 折射率灵敏度提升了近4倍。

关键词 光纤传感器; 光纤法珀微波导腔; 微波导; 双光子聚合3D打印; 折射率

中图分类号 TN253

文献标志码 A

DOI: 10.3788/AOS231441

1 引言

光纤法布里-珀罗(法珀)微腔传感器因具有体积小、稳定性好等优点, 被广泛应用于温度^[1]、应力^[2]、气压^[3]、磁场^[4]、折射率^[5]等物理量的测量。传统的光纤法珀微腔传感器的制备方法主要有熔接法、空芯光纤填充法、化学腐蚀法。

熔接法是将单模光纤与其他光纤熔接形成一个法珀微腔^[6-7]。2014年, Gao^[8]在两根标准单模光纤中间熔接超细光纤, 将两个单模光纤熔接端之间的开口空腔作为法珀微腔, 从而构成传感器用于折射率检测。熔接法由于单模光纤与特种光纤材料的不同, 熔接后容易产生大的损耗; 且某些特种光纤结构强度相对较低, 可能在熔接区域塌陷形成锥形结构, 导致制备的传感器性能不佳。空芯光纤填充法是将聚合物或液体填充至空芯光纤腔内制成法珀传感器来实现检测^[9]。2018年, Zhao等^[10]利用毛细作用, 在HCF内部镶嵌聚二甲基硅氧烷聚合物(PDMS)薄膜, 形成带有空气微腔的光纤法珀微腔传感器用于低频声压的测量, 在10~50 Hz的低频声压范围内, 其灵敏度为0.427 mV/mPa。这种基于聚合物填充法制备的光学

微腔灵敏度相对较高, 但相比于其他制备方法, 其操作相对困难, 制备重复性较差。化学腐蚀通常是将光纤拼接后使用化学试剂有选择性地腐蚀光纤制成传感器^[11]。2016年, Li等^[12]将单模光纤与光子晶体光纤(PCF)熔接后, 利用氢氟酸腐蚀PCF端面形成FP传感器并用于折射率检测, 并将其应用到lambda噬菌体DNA溶液的浓度测量。化学腐蚀法具有制作难度低、成本低等优点, 但化学腐蚀试剂通常易挥发, 容易对人体造成伤害。

针对以上问题, 本文在光纤法珀微腔干涉型传感器的微腔内引入微波导, 形成集传感和导光为一体的光纤法珀微波导腔(MWC)结构。微腔可以将光场限制在微米量级的区域内, 同时可以对腔内的微波导结构起支撑保护作用; 微波导结构可以提升整体的导光能力, 基于其强倏逝场特性可提升整体结构的折射率灵敏度。实验中, 使用飞秒激光直写双光子聚合3D打印技术直接在SMF端面打印出光纤法珀MWC结构, 其折射率灵敏度与仿真结果高度匹配。相比于传统的光纤法珀微腔结构, MWC结构不仅灵敏度得到提升, 插入损耗也显著降低。此外, 双光子聚合微纳加工技术凭借其超高的加工精度, 可以保证光纤法珀MWC

收稿日期: 2023-08-18; 修回日期: 2023-09-28; 录用日期: 2023-10-07; 网络首发日期: 2023-11-14

基金项目: 国家自然科学基金(62205051)、河北省高等学校科学技术研究项目重点项目(QN2021306)、河北省自然科学基金(F2021501011, F2020501040)

通信作者: *chenmaoqing@neu.edu.cn; **zhaoyong@ise.neu.edu.cn

制备的重复性。

2 实验原理及仿真

2.1 光纤法珀微腔传感器

将光学法珀干涉仪应用到光纤传感领域,即形成了光纤法珀微腔传感器结构,通常以SMF的端面作为干涉系统的反射端面,且光束垂直入射,此时以反射光为例,其强度 I 可表示为

$$I = I_1 + I_2 + 2\sqrt{I_1 I_2} \cos \delta, \quad (1)$$

式中: I_1 和 I_2 分别为微腔中的两个反射面的反射光强度; δ 为 I_1 和 I_2 的相位差。

$$\delta = \frac{4\pi nL}{\lambda} + \varphi_0, \quad (2)$$

式中: n 为光纤法珀微腔传感器中微腔内部介质的折射率; L 为微腔的腔长; λ 为入射光的波长; φ_0 为入射光初相位。干涉光谱的自由光谱范围(FSR) R_{FS} 可表示为

$$R_{FS} = \lambda_2 - \lambda_1 = \frac{\lambda_1 \cdot \lambda_2}{2nL}, \quad (3)$$

式中: λ_1 、 λ_2 分别为相邻两个干涉峰(或干涉谷)的峰值波长(或谷值波长)。从式(3)可以看出,当微腔内介质折射率固定时,其反射光谱的FSR随着 L 的增大而减小。通常情况下,为了获得更大的测量范围,往往需要更大的FSR,因此 L 的长度应尽量减小。但受加工精度的影响,传统的制备方式很难制备超小尺寸的微腔结构。

2.2 光纤法珀MWC传输理论分析

光纤法珀MWC腔内介质均匀,可将介质视为该波导的包层。介质中的圆形微波导结构可视为结构尺寸不同的SMF,在理论上其特征方程与SMF基本一致。与普通单模光纤不同的是,微波导结构的直径与SMF纤芯直径相差较大,对折射率的变化更加敏感,其有效折射率将随着周围介质折射率的变化而改变。2020年,Zhang等^[13]使用Rsoft仿真软件建立仿真模型,设置微波导直径从 $0.8 \mu\text{m}$ 梯度增加到 $2.2 \mu\text{m}$,并研究其在 $1.0 \sim 1.45$ 折射率范围内的灵敏度变化,发现随着波导直径减小,光波导有效折射率对周围介质折射率变化的灵敏度明显提升^[14]。在传统的光纤法珀微腔结构中引入一段空气光路或填充一段液体^[15],使得光在微腔内的传输效率降低或传感灵敏度不高。为此,本文提出一种集传感和导光为一体的光纤法珀MWC结构,使得光在微腔内部沿着微波导进行传输,同时微波导的存在使得微腔对折射率的变化更为敏感。

图1为光纤法珀MWC结构示意图,一束入射光沿单模纤芯传输,在反射面1处发生反射和透射,形成反射光1与透射光,透射光经锥形区域耦合到微波导中,再经过反射面2,形成反射光2,为了更好地将来自光纤的光耦合到微波导中,在光纤与微波导连接处设

置锥形波导耦合区域。液体样品检测时,一般微波导折射率略高于微腔内的介质折射率,满足全反射条件。锥形波导区域处会有部分光泄漏,但大部分光会沿着微波导结构进行传输,经反射面2后,反射光也会沿着微波导传输,最终经过锥形波导耦合回SMF中,形成干涉光谱。

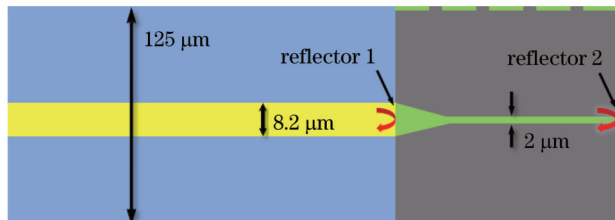


图1 光纤法珀MWC结构示意图

Fig. 1 Schematic of optical fiber Fabry-Perot MWC structure

2.3 飞秒激光双光子聚合3D打印技术

Goeppert-Mayer于1931年最先提出双光子聚合是指物质在发生双光子吸收后所引发的光聚合过程^[16]。一般情况下,聚合反应只发生在入射光波长立方 λ^3 的微小体积内,因此其加工精度可达到纳米量级。通常双光子聚合工艺应用于聚合物材料,在聚合物发生交联后再利用有机溶剂等显影液显影,得到所需要的结构。

飞秒激光双光子聚合3D打印技术(其原理图如图2所示)是将飞秒激光聚焦在透明介质内部^[17],利用激光与介质相互作用的非线性双光子吸收光聚合效应,诱发介质材料局部光学改性,通过精确控制聚焦激光与介质材料的相对移动,获得远小于衍射极限的三维结构的微加工技术^[18],这种加工方式属于点扫描,因此可以实现任意结构的精密加工。该技术是一种新的光纤制备技术^[19],其加工精度可达纳米级,同时降低了

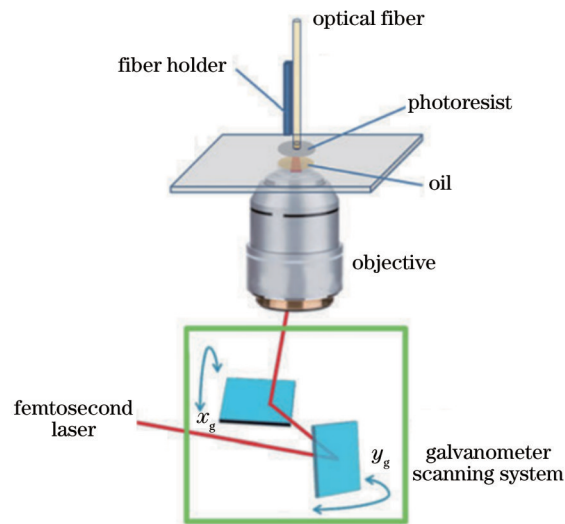


图2 飞秒激光双光子聚合3D打印技术原理图

Fig. 2 Schematic of femtosecond laser two-photon polymerization 3D printing technology

复杂光纤传感结构对特种光纤的依赖性。此外,法珀结构对微腔长度及厚度有着精确的要求,故飞秒激光 3D 打印技术对法珀微腔的制备有着极大的优势。

与传统的熔接、填充、腐蚀等工艺相比,使用双光子聚合 3D 打印技术制备光纤法珀微腔具有加工精度高、灵活性强、重复性好等优点,同时降低了复杂光纤传感结构对特种光纤的依赖性。此外,多样的可选择制备材料,也为基于飞秒激光双光子聚合 3D 打印制备不同应用场景的光纤法珀微腔提供便利。然而,双光子聚合 3D 打印微腔需要清洗内部光刻胶,所以微结构不能是封闭式的,这特点也可被巧妙应用于特殊场合的参数检测,比如 2021 年,Chen 等^[20]利用 PVA 材料的折射率随湿度变化来实现湿度检测,城堡型镂空壁增加湿敏材料与水分子的接触面积,提升传感器响应速度与灵敏度。

2.4 仿真建模分析

在本结构设计中,光纤法珀 MWC 是核心元件,承担着光信号的传输与获取任务,因此其光学传感特性将直接决定传感器的性能。为建立光纤法珀 MWC 理论模型,首先需要基于光学法珀干涉原理建立理论模型,同时为了更精确地验证结构的可行性,通过仿真软件建立仿真模型,使用有限时域差分(FDTD)法^[21]与有限元分析法(FEM)^[22]递推模拟波在时域中的传播过程以及场的分布,并通过模拟光纤法珀 MWC 的干涉光谱,研究当微波导的长度、直径、形状、有效折射率变化时,光纤法珀微腔干涉光谱的移动情况,从而优化光纤法珀 MWC 的结构设计。

微波导尺寸较小,对加工精度要求较高,因此利用传统的制备方式很难实现。基于飞秒激光双光子聚合的 3D 打印技术^[23]可以灵活、高精度地制备各种传感器。打印所需材料为光刻胶。经双光子吸收后的光刻胶折射率为 1.52~1.54,设置仿真结构的折射率为 1.53,背景折射率的变化范围为 1.333~1.337,设置光纤法珀 MWC 腔长为 50 μm,锥形波导长度为 20 μm,锥腰底直径为 8.2 μm、顶直径为 2 μm,微波导直径为 2 μm,光纤法珀 MWC 干涉光谱的折射率响应和折射率灵敏度拟合结果分别如图 3 和图 4 所示。从仿真结果可以看出,随着折射率的增加,干涉光谱特征波长出现明显的蓝移,对光谱数据进行波峰解调,仿真获得的折射率灵敏度可达 555.14 nm/RIU。

3 传感器制作及实验验证

3.1 光纤微波导腔结构制备及折射率测量

为研究波导结构对传感效果的提升,设计并制备光纤法珀 MWC 结构。为确保微波导能快速感知外界折射率的变化,微腔采用侧壁镂空的开放式结构,图 5(a)为所设计的光纤法珀 MWC 原理图(为清晰显示微波导结构,对镂空形外罩进行侧切处理)。MWC 腔长为 50 μm,微波导直径为 2 μm,锥形耦合区的最大

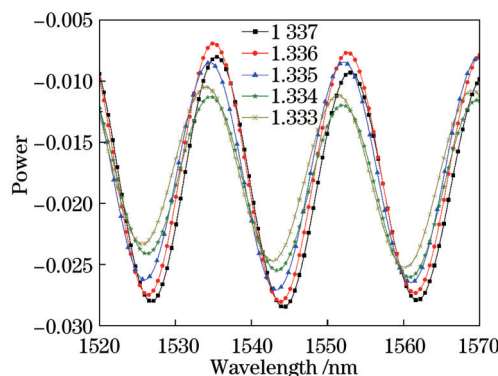


图 3 光纤法珀 MWC 光谱随折射率的变化

Fig. 3 Spectra of optical fiber Fabry-Perot MWC changed with refractive index

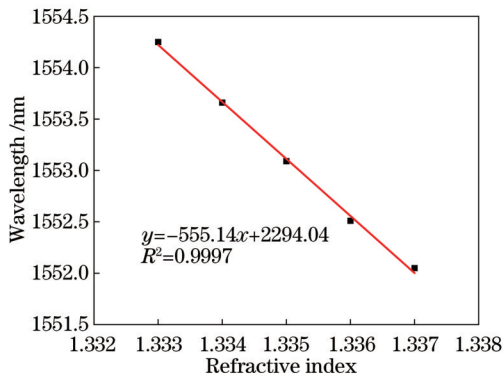


图 4 光纤法珀 MWC 折射率灵敏度线性拟合结果

Fig. 4 Linear fitting results of refractive index sensitivity of optical fiber Fabry-Perot MWC

锥腰直径为 8.2 μm。

光纤法珀 MWC 结构制备过程主要分为以下三步:1) 打印端面处理。取一根 SMF,剥除涂覆层,使用乙醇溶液擦拭干净;使用切割刀将光纤端面切割平整,将切割后的 SMF 放置在熔接机中观察,并对 SMF 端面放电清洁;将处理后的 SMF 放置在夹具中,并将夹具固定在打印设备。2) 镜头聚焦与纤芯位置确认。调整镜头位置,将镜头聚焦到光纤端面,使用 650 nm 可见光激光光源进行补光处理,并使用微位移平台摇杆调节光纤端面位置。所聚焦光斑的位置即为光纤纤芯的位置。调节微位移平台,将光纤端面调节至打印设备的中心位置。3) 结构打印。调节激光强度、频率等参数,导入打印模型图并开始打印。打印时需要实时观察打印的结构是否处于光纤端面的几何中心,是否发生倾斜、断裂等。

打印方式为增材打印,光波导结构与微波导腔是同时从结构底部(单模光纤端面)向顶部打印,打印过程完全同步能保证结构更加稳定。打印结束后,将固定光纤的夹具从打印设备中取下,将打印结构固定到载玻片上。将光纤悬空放置在载玻片上并固定。将载玻片先后插入丙二醇甲醚醋酸酯溶液和异丙醇溶液中

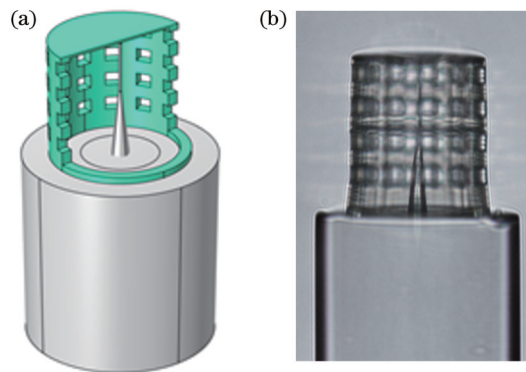


图 5 光纤法珀 MWC 结构。(a)示意图;(b)实物图

Fig. 5 Structure of optical fiber Fabry-Perot MWC.

(a) Schematic; (b) physical diagram

清洗。待结构干燥后,将其放置在显微镜下观察,实物图如图 5(b)所示。

图 6 为该结构在水中形成的反射光谱,从光谱中可以看出该结构在去离子水中形成的光谱 FSR 为 16.1 nm。对该光谱进行傅里叶变换,变换结果如图 7 所示。该结构在低频波段形成一个干涉效果良好的单峰。这也证实了在光纤法珀 MWC 结构中,微腔可以为微波导结构提供良好的抗干扰作用,在一定程度上屏蔽了外界扰动。从图 8 可以看出,随着微腔内介质折射率的增加,特征光谱逐渐向短波长方向移动,即发生蓝移。

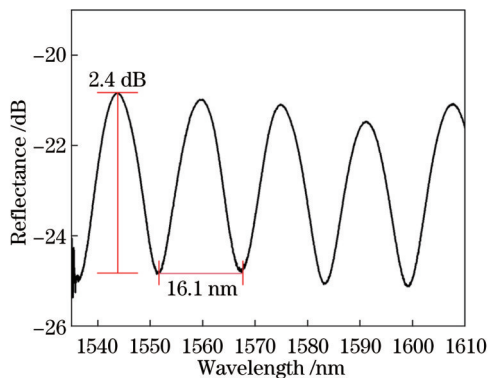


图 6 光纤法珀 MWC 结构在去离子水中的反射光谱

Fig. 6 Reflection spectrum of optical fiber Fabry-Perot MWC in deionized water

将 MWC 结构分别放在折射率在 1.3346~1.3764 范围的 12 种不同浓度的氯化钠溶液中进行实验,图 9 所示为制备的光纤法珀 MWC 结构在不同折射率溶液下的反射光谱线性拟合结果。可以看到,所设计的传感结构在 1.3346~1.3764 折射率范围内的线性度较好,灵敏度为 525.81 nm/RIU,实验获得的折射率灵敏度结果与光纤微波导微腔 FDTD 仿真结果十分接近。同时,为了验证加工技术的可重复性,使用相同的结构参数和相同的激光配置,二次制备传感探头并进行了折射率测量实验,图 10 所示为二次制备的光纤法珀

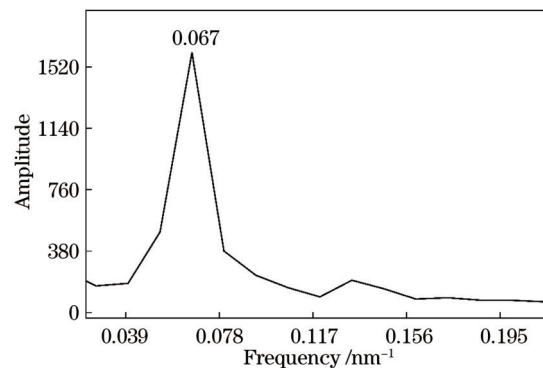


图 7 光纤法珀 MWC 结构反射光谱的傅里叶变换结果

Fig. 7 Fourier transform result of reflection spectrum of optical

fiber Fabry-Perot MWC

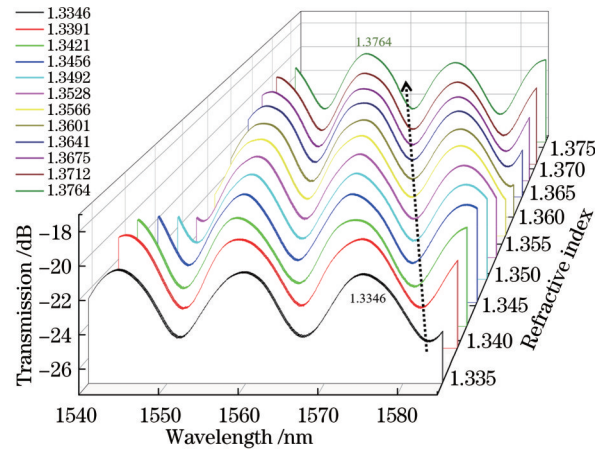


图 8 1.3346~1.3764 折射率范围内的干涉光谱变化情况

Fig. 8 Interference spectrum shifts within refractive index range of 1.3346~1.3764

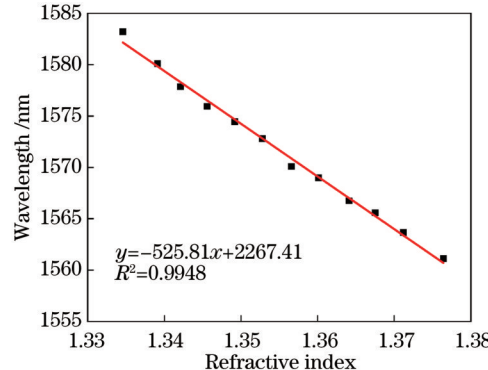


图 9 基于双光子聚合技术制备的光纤法珀 MWC 结构在不同折射率溶液下的反射光谱线性拟合结果

Fig. 9 Linear fitting results of reflection spectra of optical fiber Fabry-Perot MWC prepared by two-photon polymerization technology under different refractive index solutions

MWC 结构在不同折射率溶液下的反射光谱线性拟合结果。该传感结构在 1.3351~1.3741 折射率范围内灵敏度为 525.68 nm/RIU,与第一次实验所得灵敏度

仅差0.13 nm/RIU,足以忽略不计的灵敏度差证明了该技术的可重复性良好。

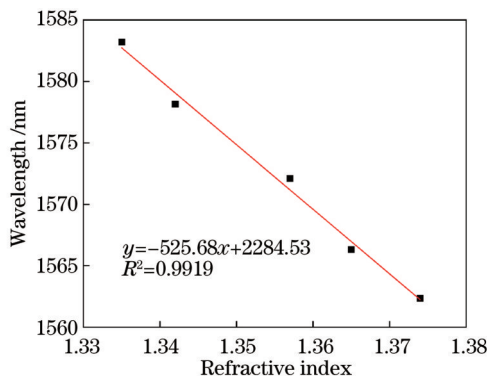


图 10 可重复性实验所用光纤法珀 MWC 结构在不同折射率溶液下的反射光谱线性拟合结果

Fig. 10 Linear fitting results of reflection spectra of optical fiber Fabry-Perot MWC structure used in repeatability experiments under different refractive index solutions

3.2 无微波导法珀微腔结构的折射率传感特性

为了验证光纤法珀 MWC 对传感结构的性能提升效果,使用双光子聚合 3D 打印技术制备了腔长同样是 50 μm 的无微波导法珀微腔结构。将该结构放置在折射率为 1.3346~1.3764 的 5 种不同浓度的氯化钠溶液中,并进行传感测量。

图 11 所示为无微波导法珀微腔结构在不同折射率溶液下干涉光谱响应情况。图 12 所示的线性拟合结果表明,无微波导法珀微腔结构的折射率灵敏度为 115.31 nm/RIU, 折射率灵敏度相较于光纤法珀 MWC 降低了 78.1%, 干涉光谱峰值降低了 8.2 dB。由此可见,在光纤法珀微腔内部耦合一根微波导确实可以提升整体结构的导光特性和折射率传感能力。

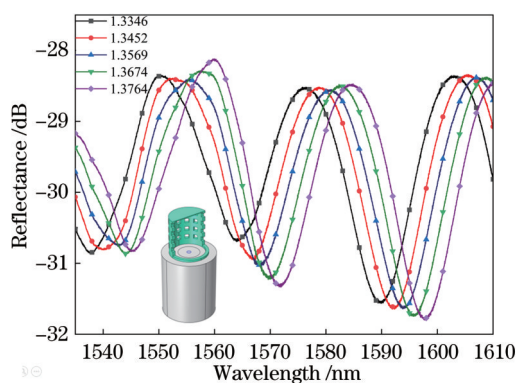


图 11 无微波导法珀微腔结构在不同折射率溶液下反射光谱, 插图为无微波导法珀微腔结构示意图

Fig. 11 Reflection spectra of waveguide-free optical fiber Fabry-Perot microcavity structure in different refractive index solutions, and the illustration shows microcavity structure without micro-waveguide

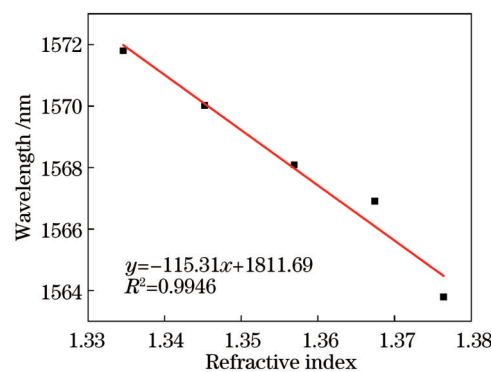


图 12 无微波导法珀微腔结构的折射率灵敏度线性拟合结果

Fig. 12 Linear fitting results of refractive index sensitivity for Fabry-Perot microcavity structure without micro-waveguide

4 结 论

基于飞秒激光双光子聚合的 3D 打印技术制备了一种新型光纤法珀微波导腔一体化传感结构,结合光纤法珀微腔的稳定性光谱与微波导的强倏逝场特性,实现了高灵敏度的折射率参数检测,在 1.3346~1.3764 折射率范围内灵敏度为 525.81 nm/RIU,与无波导法珀微腔相比,灵敏度提升了 3.56 倍,生成的干涉光谱峰值提升了 8.2 dB。这样一种样本量需求小、灵敏度高、可重复性好的光纤传感器,无疑将成为正在迅速发展的光纤传感技术、生物医学研究的强力助推剂,在生物检测相关领域具有较大的学术研究价值和良好的应用前景。

参 考 文 献

- [1] 谢佳一, 苏国帅, 李明宇, 等. 反射型法布里-珀罗腔和微环谐振腔级联的温度传感器[J]. 光学学报, 2022, 42(23): 2328002. Xie J Y, Su G S, Li M Y, et al. Temperature sensor with reflective Fabry-Perot cavity and micro-ring resonator cascaded [J]. Acta Optica Sinica, 2022, 42(23): 2328002.
- [2] 王旗, 邹辉, 韦玮. 基于偏芯熔接光纤的应力与折射率传感器[J]. 光学学报, 2017, 37(10): 1006005. Wang Q, Zou H, Wei W. Strain and refractive index sensor based on core-offset splicing fibers[J]. Acta Optica Sinica, 2017, 37(10): 1006005.
- [3] Li Z, Zhang Y X, Zhang W G, et al. High-sensitivity gas pressure Fabry-Perot fiber probe with micro-channel based on vernier effect[J]. Journal of Lightwave Technology, 2019, 37(14): 3444-3451.
- [4] Sun H Z, Jiang C Q, Tang J R, et al. High sensitivity optical fiber magnetic field sensor based on semi fixed extrinsic Fabry-Perot interferometer[J]. Optical Fiber Technology, 2022, 70: 102890.
- [5] 武洁雅, 康娟, 董洁, 等. 基于 PDMS 水滴型光纤挥发性有机化合物传感器[J]. 光学学报, 2022, 42(21): 2128001. Wu J Y, Kang J, Dong J, et al. PDMS-based drop-type optical fiber sensor for volatile organic compounds[J]. Acta Optica Sinica, 2022, 42(21): 2128001.
- [6] 徐廷廷, 杨玉强, 杨文龙, 等. 基于 PDMS 膜封装空芯光纤的级联双腔温度传感器[J]. 光学学报, 2022, 42(8): 0806004. Xu T T, Yang Y Q, Yang W L, et al. Cascaded double-cavity

- temperature sensor based on hollow fibers encapsulated by PDMS membrane[J]. *Acta Optica Sinica*, 2022, 42(8): 0806004.
- [7] Lü R Q, Li S Q, Wang W, et al. Temperature characterization of thin-walled-microsphere air-cavity fiber sensing structures[J]. *Sensors and Actuators A*, 2023, 349: 114081.
- [8] Gao S C, Zhang W G, Bai Z Y, et al. Microfiber-enabled in-line Fabry-Pérot interferometer for high-sensitive force and refractive index sensing[J]. *Journal of Lightwave Technology*, 2014, 32(9): 1682-1688.
- [9] 王超, 冯国英, 陈晓旭, 等. 空芯光子晶体光纤的塌缩及选择性液体填充[J]. 激光与红外, 2019, 49(9): 1119-1123.
Wang C, Feng G Y, Chen X X, et al. Fabrication of selective injection microstructured optical fibers[J]. *Laser & Infrared*, 2019, 49(9): 1119-1123.
- [10] Zhao Y, Chen M Q, Xia F, et al. Small in-fiber Fabry-Perot low-frequency acoustic pressure sensor with PDMS diaphragm embedded in hollow-core fiber[J]. *Sensors and Actuators A*, 2018, 270: 162-169.
- [11] Wu S N, Yan G F, Lian Z G, et al. An open-cavity Fabry-Perot interferometer with PVA coating for simultaneous measurement of relative humidity and temperature[J]. *Sensors and Actuators B*, 2016, 225: 50-56.
- [12] Li J C, Qiao X G, Wang R H, et al. Temperature-independent refractometer based on fiber-optic Fabry-Perot interferometer[J]. *Optics and Lasers in Engineering*, 2016, 79: 16-21.
- [13] Zhang D W, Wei H M, Hu H Z, et al. Highly sensitive magnetic field microsensor based on direct laser writing of fiber-tip optofluidic Fabry-Pérot cavity[J]. *APL Photonics*, 2020, 5 (7): 076112.
- [14] Reghuprasad A E, Colombero C, Godio A. Serially connected cantilever beam-based FBG accelerometers: design, optimization and testing[J]. *Sensors*, 2023, 23(6): 3188.
- [15] Wang J, Liu Z Y, Gao S R, et al. Fiber-optic anemometer based on Bragg grating inscribed in metal-filled microstructured optical fiber[J]. *Journal of Lightwave Technology*, 2016, 34(21): 4884-4889.
- [16] Göppert-Mayer M. Elementary processes with two quantum transitions[J]. *Annalen Der Physik*, 2009, 18(7/8): 466-479.
- [17] Chen M Q, He T Y, Zhao Y. Review of femtosecond laser machining technologies for optical fiber microstructures fabrication[J]. *Optics & Laser Technology*, 2022, 147: 107628.
- [18] Chen Q D, Wu D, Niu L G, et al. Phase lenses and mirrors created by laser micronanofabrication via two-photon photopolymerization[J]. *Applied Physics Letters*, 2007, 91(17): 171105.
- [19] 赵圆圆, 罗海超, 梁紫鑫, 等. 光聚合微纳3D打印技术的发展现状与趋势[J]. 中国激光, 2022, 49(10): 1002703.
Zhao Y Y, Luo H C, Liang Z X, et al. Micro-nano 3D printing based on photopolymerization and its development status and trends[J]. *Chinese Journal of Lasers*, 2022, 49(10): 1002703.
- [20] Chen M Q, Zhao Y, Wei H M, et al. 3D printed castle style Fabry-Perot microcavity on optical fiber tip as a highly sensitive humidity sensor[J]. *Sensors and Actuators B*, 2021, 328: 128981.
- [21] Singh L, Agrawal N, Saha C, et al. A plus shaped cavity in optical fiber based refractive index sensor[J]. *IEEE Transactions on NanoBioscience*, 2022, 21(2): 199-205.
- [22] Zhang P, Wang S, Jiang J F, et al. A fiber-optic extrinsic Fabry-Perot hydrophone based on Archimedes spiral-type sensitive diaphragm[J]. *IEEE Sensors Journal*, 2022, 22(23): 22654-22660.
- [23] Hadibrata W, Wei H M, Krishnaswamy S, et al. Inverse design and 3D printing of a metalens on an optical fiber tip for direct laser lithography[J]. *Nano Letters*, 2021, 21(6): 2422-2428.

Fabrication and Sensing Characteristics of Optical Fiber Fabry-Perot Micro-Waveguide Cavity Based on Two-Photon Polymerization 3D Printing

Chen Maoqing^{1,2*}, Liu Siyuan^{1,3}, Cai Lu^{1,3}, Liu Qiang^{1,3}, Zhao Yong^{1,2,3**}

¹College of Information Science and Engineering, Northeastern University, Shenyang 110819, Liaoning, China;

²State Key Laboratory of Synthetical Automation for Process Industries, Northeastern University, Shenyang 110819, Liaoning, China;

³Hebei Key Laboratory of Micro-Nano Precision Optical Sensing and Measurement Technology, Qinhuangdao 066004, Hebei, China

Abstract

Objective Optical fiber Fabry-Perot microcavity sensor has the advantages of small size and good stability, and it is widely used in the measurement of temperature, magnetic field, refractive index, and other physical quantities. However, the traditional processing method has many drawbacks and limitations. For example, the fusion method of single-mode fibers and special fibers may cause the fusion area to collapse and form a conical structure, resulting in poor performance of the prepared sensor; the operation of the hollow-core fiber filling method is difficult, and the preparation repeatability is poor; the chemical reagents of chemical corrosion method are easy to cause harm to the human body. The femtosecond laser two-photon polymerization 3D printing technology adopted in this paper has the advantages of high processing precision, strong flexibility, and high repeatability and can cope with more complex conditions to achieve structure preparation. In addition, the optical fiber Fabry-Perot microcavity sensor is widely used in refractive index sensing, but due to the introduction of a section of air optical path, its light conduction ability is relatively insufficient, and the insertion loss is large. In this paper, the optical micro-waveguide is introduced to form the integrated sensing and guiding optical

fiber Fabry-Perot micro-waveguide cavity. The Fabry-Perot microcavity can limit the light field to the micron range and support and protect the micro-waveguide structure. Meanwhile, micro-waveguides not only ensure good optical conductivity of the structure but also further enhance the refractive index sensitivity of the overall structure based on their strong evanescent field characteristics.

Methods The micro-waveguide Fabry-Perot cavity structure is designed by COMSOL and simulated by finite difference time domain method and finite element method. The simulation results show that the refractive index sensitivity of the proposed structure can reach 555.14 nm/RIU in the range of 1.333–1.337 (Fig. 3). The structure is prepared by femtosecond laser two-photon polymerization 3D printing after setting the printing parameters. First, the fiber coating layer is removed; the flat single-mode fiber core end face with a cutter is cut out, and it is cleaned with a welding machine. Second, the optical fiber is fixed to the printer position, and the lens is focused on the optical fiber end face. Third, the optical fiber end face is adjusted to the center position of the printing equipment for printing. Fourth, the structure is cured using propylene glycol methyl ether acetate solution and isopropyl alcohol solution (Fig. 4).

Results and Discussions The reflection spectrum of the printed structure in water is observed by the optical spectrum analyzer. It can be seen that the free spectrum range (FSR) of the structure formed in deionized water is 16.1 nm. The spectral Fourier transform results show that the structure forms a single peak with a good interference effect in the low-frequency band (Fig. 5). It is also confirmed that the micro-waveguide structure can play a good anti-interference role in the optical fiber structure and shield the external disturbance to a certain extent. The structures are placed in 12 sodium chloride solutions with different concentrations in the refractive index range of 1.3346–1.3764 for experiments, and the linear fitting results of the reflection spectra show that the sensing structure has good linearity and sensitivity of 525.81 nm/RIU in the refractive index range of 1.3346–1.3764 (Fig. 6 and Fig. 7). To verify the improvement effect of micro-waveguides on the sensing performance of Fabry-Perot microcavities, a waveguide-free optical fiber Fabry-Perot microcavity with the same cavity length is prepared using 3D printing technology, and the structure is placed in different concentrations of sodium chloride solution in the refractive index range of 1.3346–1.3764; the linear fitting results show that the refractive index sensitivity of the microcavity structure without micro-waveguide is 115.31 nm/RIU. It is not difficult to see that with the support of a micro-waveguide, the refractive index sensitivity of the optical fiber Fabry-Perot microcavity has increased by nearly 4 times, and the peak interference spectrum has increased by 8.2 dB (Fig. 9).

Conclusions Based on femtosecond laser two-photon polymerization 3D printing technology, a novel optical fiber Fabry-Perot micro-waveguides cavity integrated sensing structure is prepared in this paper. By combining the stability spectrum of fiber Fabry-Perot micro-cavity and the strong evanescent field characteristics of the optical micro-waveguide, the refractive index parameter detection with high sensitivity is realized. In the refractive index range of 1.3346–1.3764, the sensitivity is 525.81 nm/RIU, which is 3.56 times higher than that of the waveguide-free Fabry-Perot microcavity, and the peak value of the generated interference spectrum is increased by 8.2 dB. Such a fiber optic sensor with a small sample size, high sensitivity, and good repeatability will undoubtedly become a powerful booster for the rapidly developing fiber optic sensing technology and biomedical research and has a wide range of academic research value and application prospects in biodetection-related fields.

Key words optical fiber sensor; optical fiber Fabry-Perot micro-waveguide cavity; micro-waveguide; two-photon polymerization 3D printing; refractive index